Amino Acids (2011) 41:1103–1112
DOI 10.1007/s00726-010-0548-9

ORIGINAL ARTICLE

Phage display peptide probes for imaging early response to bevacizumab treatment

Qizhen Cao · Shuanglong Liu · Gang Niu · Kai Chen · Yongjun Yan · Zhaofei Liu · Xiaoyuan Chen

Received: 16 February 2010 / Accepted: 25 February 2010 / Published online: 16 March 2010

Abstract Early evaluation of cancer response to a therapeutic regimen can help increase the effectiveness of treatment schemes and, by enabling early termination of ineffective treatments, minimize toxicity, and reduce expenses. Biomarkers that provide early indication of tumor therapy response are urgently needed. Solid tumors require blood vessels for growth, and new anti-angiogenic agents can act by preventing the development of a suitable blood supply to sustain tumor growth. The purpose of this study is to develop a class of novel molecular imaging probes that will predict tumor early response to an anti-angiogenic regimen with the humanized vascular endothelial growth factor antibody bevacizumab. Using a bevacizumab-sensitive LS174T colorectal cancer model and a 12-mer bacteriophage (phage) display peptide library, a bevacizumab-responsive peptide (BRP) was identified after six rounds of biopanning and tested in vitro and in vivo. This 12-mer peptide was metabolically stable and had low toxicity to both endothelial cells and tumor cells. Near-infrared dye IRDye800-labeled BRP phage showed strong binding to bevacizumab-treated tumors, but not to untreated control LS174T tumors. In addition, both IR-Dye800- and ^{18}F-labeled BRP peptide had significantly higher uptake in tumors treated with bevacizumab than in controls treated with phosphate-buffered saline. Ex vivo histopathology confirmed the specificity of the BRP peptide to bevacizumab-treated tumor vasculature. In summary, a novel 12-mer peptide BRP selected using phage display techniques allowed non-invasive visualization of early responses to anti-angiogenic treatment. Suitably labeled BRP peptide may be potentially useful pre-clinically and clinically for monitoring treatment response.

Keywords Phage display · Angiogenesis · Therapy response · Bevacizumab · Molecular imaging

Introduction

It was found several decades ago that tumors implanted into isolated perfused organs failed to grow beyond a few millimeters in diameter without angiogenesis (Browder et al. 2000; Holash et al. 1999). Consequently, anti-angiogenic and anti-vascular agents have been intensively investigated for tumor therapy. By targeting tumor vasculature, anti-angiogenic agents do not need to overcome the physiological barriers within tumors (Jain 1998). In addition, local and circulating endothelial cells are considered genetically stable, so they will presumably resist changes by genetic and epigenetic mechanisms (Browder et al. 2000). Bevacizumab, a humanized monoclonal antibody directed against human vascular endothelial growth factor (VEGF), was the first antibody drug developed as an inhibitor of angiogenesis to be approved by the Food and Drug Administration (FDA) (Ferrara 2004; Hurwitz et al.

Electronic supplementary material The online version of this article (doi:10.1007/s00726-010-0548-9) contains supplementary material, which is available to authorized users.

Q. Cao · S. Liu · Z. Liu · X. Chen
Molecular Imaging Program at Stanford (MIPS), Department of Radiology and Bio-X Program, Stanford University School of Medicine, 1201 Welch Road, Stanford, CA 94305, USA

G. Niu · K. Chen · Y. Yan · X. Chen (✉)
Laboratory of Molecular Imaging and Nanomedicine (LOMIN), National Institute of Biomedical Imaging and Bioengineering (NIBIB), National Institutes of Health (NIH), 31 Center Drive, Suite 1C14, Bethesda, MD 20892-2281, USA
e-mail: shawn.chen@nih.gov

2004; Kerbel 2006). Bevacizumab neutralizes all isoforms of human VEGF and inhibits VEGF-induced proliferation of endothelial cells. A combination of bevacizumab with paclitaxel resulted in marked suppression of tumor growth both in the CWR22R androgen-independent xenograft model of prostate cancer and in the OVCAR3 ovarian tumor model (Fox et al. 2002; Hu et al. 2002). It has also been reported that bevacizumab could reverse the protective effect on endothelial cells of the high levels of VEGF produced by the tumor (Sweeney et al. 2001).

The conventional "gold standard" to evaluate therapeutic response is tumor volume change. Clinical trials with cytotoxic chemotherapeutic agents have mainly used morphological imaging—in particular, computed tomography (CT) and magnetic resonance imaging (MRI), according to the Response Evaluation Criteria in Solid Tumors (RECIST) introduced in the year 2000 (Jaffe 2006)—to provide indices of therapeutic response. However, anti-angiogenic agents are typically cytostatic rather than cytotoxic, leading to a stop or delay in tumor progression, rather than tumor shrinkage. Thus, tumor volume is an insensitive indicator for evaluation of therapeutic efficacy, and moreover may take months or years to assess. Currently, microvessel density (MVD) is the most commonly used end-point for assessing anti-angiogenic treatment in clinical studies. MVD is measured from biopsies taken before and at one or more times after treatment is complete, using a variety of immunohistochemical vascular markers to identify the vessels (Willett et al. 2004). However, measurement of MVD is problematic for assessing the vascular efficacy of anti-angiogenic agents (Fujio and Walsh 1999), since blocking of angiogenesis may be accompanied by a proportional reduction in tumor growth that would not result in a net change in MVD. Besides, vessel counts and/or density measurements may remain unchanged even in the event of effective therapy (Hlatky et al. 2002). A similar problem has also been found with non-invasive imaging methods for measuring functional vascular volume, such as positron emission tomography (PET) studies with ^{15}O-oxygen (Miller et al. 2005), contrast-enhanced ultrasound (CEU) (Hughes et al. 2006), and dynamic contrast-enhanced MRI (DCE-MRI) (Padhani 2003), i.e., the absence of an effect on vascular volume by non-invasive imaging cannot be interpreted as the absence of anti-angiogenic effect (Tozer 2003).

Biomarkers have great value in early efficacy and safety evaluations, disease diagnosis/staging, indicating disease prognosis, and prediction/monitoring of clinical response to a given intervention (Atkinson et al. 2001). Recently, molecular imaging with biological markers has emerged to provide valuable information at the structural/functional and/or molecular level. Compared with relatively large biomolecules, such as antibodies and proteins, small peptides have advantages as potential probes for molecular imaging. The display of peptide libraries on the surface of bacteriophage (phage) offers a way of searching for peptides with specific binding properties. Phage display peptide libraries are commonly used to obtain defined peptide sequences that interact with a particular molecule. The strength of this technology is its ability to identify interactive regions of proteins and other molecules without preexisting notions about the nature of the interaction. Especially, in vivo phage display selection procedures offer an advantage over in vitro screening protocols in that phages can be selected based on desired pharmacokinetic properties, including delivery and tumoral accumulation. Recently, in vivo phage display has been explored as a means to identify phage and corresponding peptides with optimal tumor-targeting properties in the context of living animals (Han et al. 2008). Moreover, many of these peptides bind to endothelial cell markers, but not directly to tumor cells (Arap et al. 1998; Pasqualini and Ruoslahti 1996). Thus, it is possible to obtain peptide sequences reflecting molecular changes of endothelial cells upon anti-angiogenesis therapy. Using the bevacizumab-sensitive LS174T colorectal cancer model and in vivo biopanning of a 12-mer phage display peptide library, in this study, we developed a class of novel molecular imaging probes to predict early responses by tumors to bevacizumab treatment.

Materials and methods

Cell lines

The LS174T human colorectal cancer cell line was purchased from American Type Culture Collection (ATCC) and was maintained in medium supplemented with 10% FCS and 1% penicillin–streptomycin as ATCC recommends. Normal human umbilical vein endothelial cells (HUVECs) and relevant culture medium were purchased from PromoCell (Germany).

Chemicals

Bevacizumab (trade name Avastin®) was purchased from Genentech/Roche. IRdye800-NHS and Cy5.5-NHS were from Li-Cor and GE Healthcare, respectively. Fluorescein isothiocyanate (FITC)-labeled tomato lectin was from Thermo Fisher Scientific (Rockford, IL). The bevacizumab-responsive peptide (BRP) peptide was synthesized by Peptides International.

Animal models

All animal experiments were performed in compliance with the guidelines for the care and use of research animals

established by the Stanford University's Animal Studies Committee. Female athymic nude mice (nu/nu) were obtained from Harlan (Indianapolis, IN) at 6–8 weeks of age and were kept under sterile conditions. The LS174T cells were harvested and suspended in sterile phosphate-buffered saline (PBS) at a concentration of 5×10^7 viable cells/ml. Viable tumor cells (5×10^6) in sterile PBS (100 µl) were injected subcutaneously into the right shoulder. Tumor growth was followed by caliper measurements of perpendicular measures of the tumor. The tumor volume was estimated by the formula: tumor volume $= ab^2/2$, where a and b were the tumor length and width, respectively, in mm.

Tumor growth study

When palpable tumors (150–200 mm^3) were present in all animals, mice were randomly divided into two groups ($n = 10$ per group). Cancer therapy response was evaluated in LS174T human colorectal cancer model. The mice were injected intraperitoneally with 20 mg/kg of bevacizumab every other day for a total of three doses. The mouse body weight and tumor volume were measured every 3 days for up to 20 days before killing.

Biopanning phage-displayed libraries

We conducted in vivo biopanning with phage-displayed peptide libraries (Ph.D.-12™ phage display peptide library, New England Biolabs Inc.). The phage-displayed peptide library represents 1×10^9 independent clones of phages expressing random 12-mer peptides that are displayed on M13 phages. After the tumor-bearing mice were treated, phage libraries were administered by intracardiac injection. The amplified phages were partially purified by polyethyleneglycol (PEG) precipitation and resuspended in tris-buffered saline (TBS) for the next round of biopanning. After six rounds of biopanning, single plaques from soft agar were isolated. The peptide sequences were deduced from the decoded DNA information.

Phage labeling

Phages were labeled with a near-infrared dye IRdye800-NHS or Cy5.5. Phages (1×10^{12} pfu) were resuspended in 100 µl of 0.3 M $NaHCO_3$ (pH 8.6) solution containing 0.1 mg/ml fluorochrome-hydroxy-succinimide ester. The phage/fluorochrome reaction was allowed to continue for 1 h at room temperature in the dark. The volume of the labeled phage was then brought up to 1 ml with Dulbecco's phosphate-buffered saline (DPBS), and the phage was purified by PEG precipitation. Fluorochrome-labeled phage was then resuspended in 200 µl of DPBS and titered to determine plaque-forming units, and the concentration of fluorochrome was determined spectrophotometrically (Kelly et al. 2006).

Metabolic stability of BRP peptide

Nude mice bearing LS174T tumor xenografts were intravenously injected with 3.7 MBq of ^{18}F-FP-BRP. Urine samples were collected 1 h after tracer injection and analyzed by HPLC.

Toxicity of BRP on cell viability by MTT assay

MTT [3-(4,5-dimethylthiazol-2yl)-2,5-diphenyltetrazolium bromide; ATCC] assays were used to measure cell viability. Three thousand tumor cells or HUVECs were seeded per well in a 96-well plate and allowed to incubate for 24 h. After incubation with various concentrations of peptide BRP for 48 h, 10 µl of MTT reagent was added to each well. Four hours later, when the purple precipitate became visible, the supernatant was discarded, and 100 µl of DMSO was added to each well and the plate was shaken in the dark for 10 min at room temperature. The absorbance at 570 nm was then measured using a microplate reader (Tecan).

Near-infrared fluorescence imaging

The tumor-bearing mice (with or without bevacizumab treatment) were injected intravenously with appropriately labeled phages or BRP peptide (1 nmol dye/mouse). Two-dimensional NIR fluorescence images were acquired at various time points after injection using a Maestro in vivo imaging system (CRI, Woburn, MA; IRDye800 excitation = 735 nm, emission = 780 nm long pass).

Histologic analysis

Bevacizumab-treated LS174T tumor mice were injected with 1 nmol of Cy5.5-BRP. After 4-h blood circulation, the mice were injected with 200 µg FITC-labeled tomato lectin. The mice were killed 10 min later, and the tumors collected and made into frozen tissue blocks. These tumor specimens were subsequently sectioned with a thickness of 10 µm. Fluorescence pictures were taken under a Zeiss microscope using FITC and Cy5.5 filter settings separately. Merged pictures were made using MetaMorph.

Radiochemistry

Semipreparative reversed-phase high-performance liquid chromatography (RP-HPLC) using a Vydac protein and peptide column (218TP510; 5 µm, 250 × 10 mm) was

performed on a Dionex 680 chromatography system with a UVD 170U absorbance detector and model 105S single-channel radiation detector (Carroll & Ramsey Associates). The recorded data were processed using Chromeleon version 6.50 software. With a flow rate of 5 ml/min, the mobile phase was changed from 95% solvent A [0.1% trifluoroacetic acid (TFA) in water] and 5% B [0.1% TFA in acetonitrile (MeCN)] (0–2 min) to 35% solvent A and 65% solvent B at 32 min. Analytical HPLC had the same gradient system, except that the flow rate was 1 ml/min with a Vydac protein and peptide column (218TP510; 5 μm, 250 × 4.6 mm). The UV absorbance was monitored at 218 nm and the identification of the peptides was confirmed based on the UV spectrum acquired using a PDA detector. C_{18} Sep-Pak cartridges (Waters) were pretreated with ethanol and water before use.

FP-BRP was synthesized as follows: *O*-(*N*-succinimidyl)-1,1,3,3-tetramethyluronium tetrafluoroborate (TSTU, 17.6 mg, 58.5 μmol) was added to a solution of 2-fluoropropionic acid (7.8 mg, 84.5 μmol) in 0.5 ml anhydrous MeCN. The pH of the solution was adjusted to 8.5–9.0 by *N*,*N*-diisopropylethylamine (DIPEA). The reaction mixture was stirred at room temperature for 0.5 h and then BRP (3 μmol) in DMF was added in one aliquot. After being stirred at room temperature for 2 h, the product FP-BRP was isolated by semipreparative HPLC. The collected fractions were combined and lyophilized to a white fluffy powder. FP-BRP was obtained in 82% yield with 22-min retention time on analytical HPLC. MALDI-TOF-MS was *m*/*z* 1,522.1 for $[MH]^+$ ($C_{68}H_{102}FN_{20}O_{19}$ calculated molecular weight 1,522.7).

The labeling precursor 4-nitrophenyl 2-^{18}F-fluoropropionate (^{18}F-NFP) was synthesized as previously reported (Liu et al. 2009). ^{18}F-FP-BRP was synthesized as follows: BRP (1.0 μmol) and DIPEA (20 μl) were added to ^{18}F-NFP in anhydrous dimethyl sulfoxide (DMSO, 200 μl). The reaction mixture was allowed to incubate at 60°C for 20 min. After dilution with 2 ml of 1.0% TFA water, the mixture was injected into the semipreparative HPLC. The collected fractions containing ^{18}F-FP-BRP were combined and rotary evaporated to remove MeCN and TFA. ^{18}F-FP-BRP was obtained in 15 ± 4% yield ($n = 4$). The activity was then reconstituted in normal saline and passed through a 0.22 μm Millipore filter into a sterile multidose vial for in vivo experiments.

Small animal PET imaging

A detailed procedure for PET imaging has been reported earlier (Li et al. 2008). Briefly, PET scans were performed using a microPET R4 rodent model scanner (Siemens Medical Solutions). Mice were injected with about 100 μCi of ^{18}F-FP-BRP or ^{18}F-FDG via tail vein under isoflurane anesthesia and 3–5-min PET scans were performed at 1- and 4-h postinjection (p.i.). The images were reconstructed by a two-dimensional ordered subsets expectation maximum (OSEM) algorithm with no attenuation or scatter correction. For each microPET scan, regions of interest (ROIs) were drawn over the tumor using vendor software ASI Pro 5.2.4.0 on decay corrected whole-body coronal images. Assuming a tissue density of 1 g/ml, the ROIs were converted to MBq/g/min using a conversion factor, and then divided by the administered activity to obtain an imaging ROI-derived percent injected dose per gram (%ID/g).

Statistical analyses

Statistical significance was determined by one-way ANOVA using an SPSS (10.0) statistics package. P value <0.05 was considered significant.

Results

Isolation and identification of bevacizumab-treated tumor-homing peptides by in vivo phage display

To determine the anti-tumor effect of bevacizumab in vivo, female athymic nude mice bearing LS174T tumor were randomly divided into two groups ($n = 10$ per group) and treated with vehicle (saline) or bevacizumab (20 mg/kg every other day, by intraperitoneal injection, for a total of 3 doses). As shown in Fig. 1a, the bevacizumab therapy was associated with a significant delay of LS174T tumor growth, with a difference in tumor size from that of the controls becoming distinguishable 10 days after treatment was initiated ($P < 0.05$). No significant body weight difference was observed between the control and the treatment groups (data not shown).

To select peptides that home to bevacizumab-treated tumor, phages were injected intracardiacally in bevacizumab-treated LS174T tumor-bearing mice, recovered from the treated tumor, amplified repeatedly in vitro, and re-injected to obtain sufficient enrichment. Six rounds of biopanning were conducted prior to the isolation of the individual phage clones for DNA sequences [supporting information (SI) Fig. S1]. Sixty individual phage clones were randomly picked from the last round of screening, and DNA sequencing was conducted. The obtained DNA sequences were translated into the corresponding peptide sequences listed in Table 1. One phage peptide LLADTTHHRPWT was found to be dominantly enriched in the bevacizumab-treated tumors. LLADTTHHRPWT-displaying phage was thus chosen for further characterization as an indicator of responsiveness to bevacizumab.

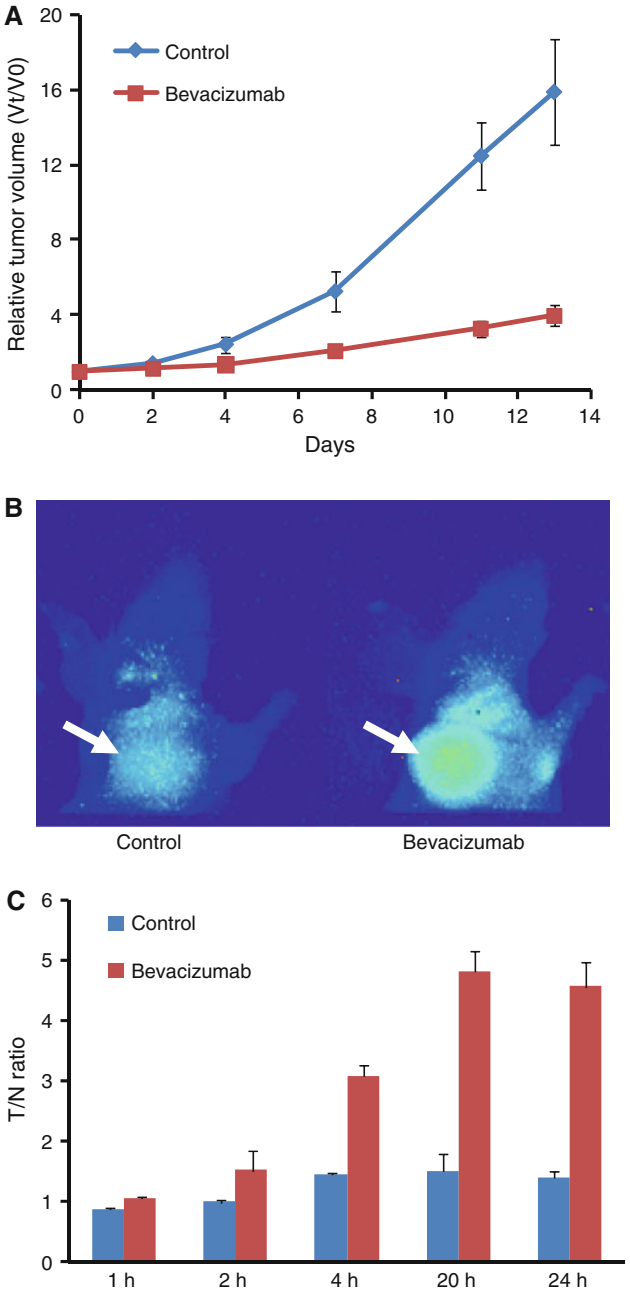

Fig. 1 **a** Bevacizumab treatment (3 doses, 20 mg/kg every other day) delayed LS174T human colorectal cancer tumor growth in a nude mouse model, with the relative tumor volume (V_t/V_0) significantly lower than that of the saline control group at day 10 following initiation of treatment ($n = 10$ per group, $P < 0.05$). **b** Representative near-infrared fluorescence images at 24 h after intravenous injection of IRDye800-labeled LLADTTHHRPWT phages (1 nmol dye per mouse) showed prominent tumor phage particle accumulation in bevacizumab-treated, but not saline control, mice. Mice were imaged 1 day after the three doses of bevacizumab (the fifth day following the start of treatment), at which time no difference in tumor volume between the treatment and control groups was found. **c** Tumor-to-normal tissue (T/N) ratios of the 2D optical images at 1, 2, 4, 20, and 24 h after administration of optically labeled phage particles

Table 1 Percentage of phage peptide-targeting sequences

Sequence	Percentage
LLADTTHHRPWT	50
SVSVGMKPSPRP	10
LLADTTHHRPWP	8.3
LLADATHHSPWP	8.3
HSVSNIRPMFPS	4.2
SVSEGTHPSPRP	4.2

Near-infrared fluorescent dye IRDye800-labeled LLADTTHHRPWT-displaying phages, injected intravenously, were found to accumulate in bevacizumab-treated, but not saline control, tumors (Fig. 1b, c). In addition, histological detection of phage particles in tumor tissues with Cy5.5-labeled LLADTTHHRPWT phage showed that bevacizumab-treated tumor tissues had much more phage homing than saline control tumor tissues (Fig. S2). The homologous peptide was denoted as BRP.

Metabolic stability and toxicity of BRP peptide

Cytotoxicity of BRP peptide in vitro and metabolic stability in vivo was assessed, before BRP peptide was used for in vivo assessment of bevacizumab treatment efficacy. For a study of cellular toxicity, HUVECs and LS174T human colorectal cancer cells were subjected to a colorimetric MTT (3-[4,5-dimethylthiazol-2yl]-2,5-diphenyltetrazolium bromide) assay after adding BRP. Figure 2a shows that BRP had little effect on the two cell lines. Even when the BRP peptide concentration was as high as 300 μg/ml, these cells retained good viability after 48-h exposure (HUVEC, 92.2 ± 2.4%; LS174T, 98.3 ± 12.1%). To determine the metabolic stability of BRP peptide, radio-HPLC of ^{18}F-labeled BRP peptide was conducted in the mouse urine at 1-h time point after intravenous injection. The representative HPLC profiles of the reference compound ^{18}F-FP-BRP in PBS buffer and the urine sample are shown in Fig. S3. Pure ^{18}F-FP-BRP had a retention time of about 22 min (Fig. S3A). There was about 90% intact ^{18}F-FP-BRP in the urine at the 1-h time point and several minor peaks with different retention times (Fig. S3B), indicating good metabolic stability of this linear 12-mer peptide in vivo.

BRP peptide targets to bevacizumab-treated tumors

In comparison to the phage particles, peptides offer several advantages, including rapid clearance from the circulation and good contrast, better tissue penetration, less chance of immune reaction, and less possibility of liver and bone

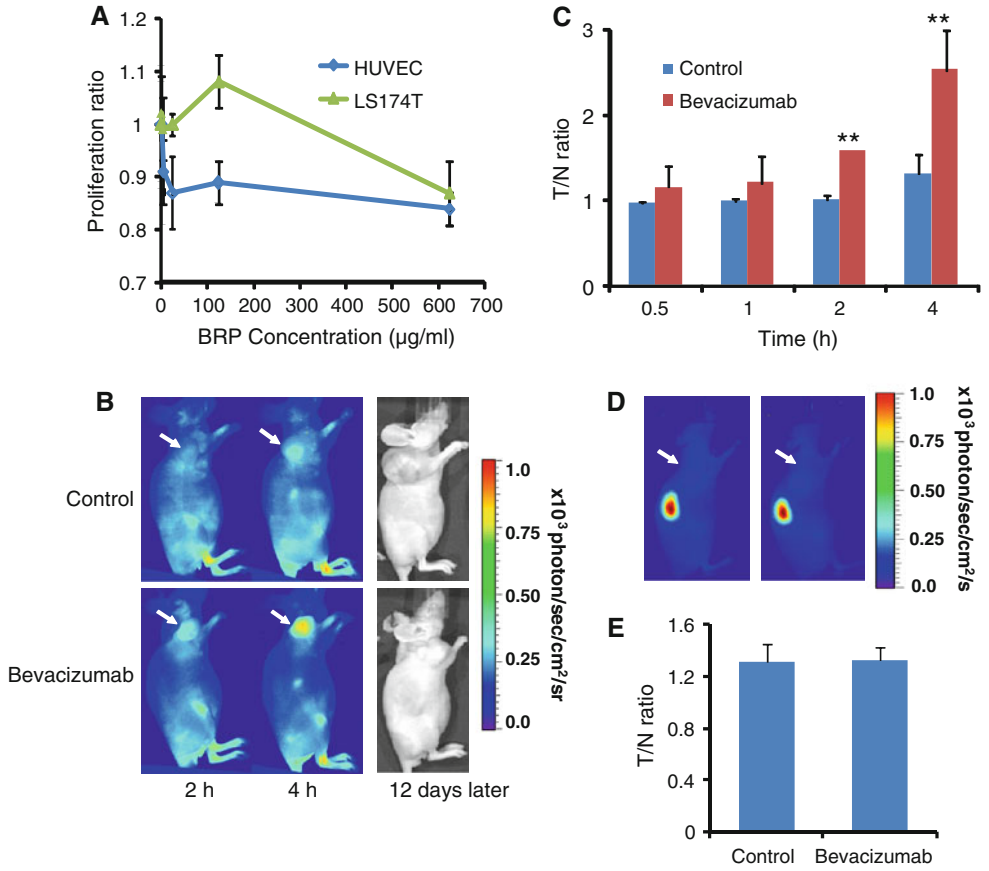

Fig. 2 **a** Colorimetric MTT (3-[4,5-dimethylthiazol-2yl]-2,5-diphenyltetrazolium bromide) assay showed that the BRP had little effect on proliferation of the LS174T colorectal cancer cells and human umbilical vein endothelial cells (HUVECs) ($n = 6$). **b** Representative near-infrared fluorescence images at 2 and 4 h after intravenous injection of IRDye800-labeled LLADTTHHRPWT peptide (IRDye800-BRP) (1 nmol dye/mouse). LS174T tumor mice were imaged 1 day after three doses of bevacizumab treatment. IRDye-BRP showed good tumor/background contrast in bevacizumab-treated, but not in saline control mice, at which time there were no differences in tumor volume between the two groups. Photos of the same mice at 12 days after the optical imaging show that the BRP imaging successfully predicted treatment outcomes. **c** Tumor-to-normal tissue (T/N) ratios of the 2D optical images at 0.5, 1, 2 and 4 h after the administration of optically labeled BRP peptide. $^{**}P < 0.01$. **d** Representative near-infrared fluorescence images at 4 h after intravenous injection of an IRdye800-labeled scrambled peptide WTLRPTLHTDHA (1 nmol dye/mouse). LS174T tumor mice were imaged 1 day after a course of three doses of bevacizumab treatment. The scrambled peptide showed rapid renal clearance and virtually no tumor contrast in either bevacizumab-treated or saline control mice. **e** T/N ratios of the 2D optical images at 4 h after the administration of IRDye800-labeled scrambled peptide

marrow toxicity. After the initial optical imaging showed that dye-labeled BRP phage specifically bound to bevacizumab-treated LS174T tumor (Fig. 1), we sought to determine whether BRP would bind to bevacizumab therapy-treated tumors in the same way.

The synthesis of dye conjugates of BRP followed our previously reported general procedure (Wu et al. 2006). Bevacizumab-treated or vehicle-treated LS174T tumor-bearing mice were injected with IRDye800-BRP conjugate (1 nmol/mouse). After injection, the contrast between bevacizumab-treated tumor and normal tissue immediately increased and was significantly higher than the vehicle-treated LS174T tumor model at 2- and 4-h time points (Fig. 2b). The tumor-to-normal tissue (T/N) ratios were 1.58 ± 0.01 at 2 h and 2.53 ± 0.46 at 4 h for bevacizumab-treated, significantly higher than those of the vehicle-treated tumors (1.01 ± 0.05 at 2 h and 1.31 ± 0.22 at 4 h, respectively) ($P < 0.01$, Fig. 2c). At the time of imaging studies (5 days following the initiation of bevacizumab treatment), there were no significant differences in tumor volume between bevacizumab-treated (312.9 mm^3) and vehicle-treated (331.4 mm^3) tumors (Fig. 1a). Figure 2b also shows the photos of the same mice at 12 days after the optical imaging was performed (2,749.9 mm^3 for the control mice and 476.6 mm^3 for the bevacizumab-treated mice). These results unarguably illustrated that the BRP peptide could predict the cancer response to anti-angiogenic therapy in an early phase of treatment.

On the contrary, a scrambled peptide (WTLRPTLHT-DHA) with IRDye800 failed to show tumor contrast in either the control or bevacizumab-treated LS174T tumors (Fig. 2d). The T/N ratios were 1.31 ± 0.13 and 1.32 ± 0.11 at the 4-h time point after intravenous injection of 1 nmol of the scrambled peptide dye conjugate for the control- and bevacizumab-treated mice, respectively (Fig. 2e). It is also noticeable that the scrambled peptide was cleared through the kidneys much faster than the BRP peptide, showing little retention of the scrambled peptide in the rest of the body at the 4-h time point.

BRP peptide targets bevacizumab-affected tumor vasculature

To further characterize the histologic binding pattern and distribution of BRP peptide within tumors, we injected Cy5.5-BRP conjugate into bevacizumab-treated LS174T tumor-bearing mice. After the distribution of the dye conjugate for 4 h, the mice were then injected with FITC-labeled tomato lectin. After circulation for 20 min, the mice were killed and the LS174T tumor was collected, frozen and cut into slices (Hsu et al. 2006). Figure 3 shows that BRP peptide binds specifically to bevacizumab-treated microvascular tumor endothelial cells. On the contrary, no binding of Cy5.5-BRP to control tumor vasculature was found (data not shown). In addition, BRP peptide does not bind to VEGF, bevacizumab, or VEGF/bevacizumab complex (Fig. S4). HUVEC co-culture with LS174T tumor cells in a Transwell® culture system showed prominent HUVEC cell uptake of Cy5.5-BRP pretreated with bevacizumab. HUVECs alone, with or without bevacizumab treatment, had no binding with Cy5.5-BRP (Fig. S5).

^{18}F-FDG and ^{18}F-FP-BRP PET imaging

^{18}F-FDG PET has been used routinely in both clinical and pre-clinical studies to measure glucose metabolism and, thereby, to evaluate stages of tumor progression and efficacy of therapeutic intervention (Gambhir et al. 2001). We carried out ^{18}F-FDG small animal PET scans on an LS174T tumor model on the same day as ^{18}F-FPP-BRP peptide administration (24 h after the third dose bevacizumab, i.e., 5 days following the start of treatment). The heart had prominent uptake of ^{18}F-FDG due to the constant beating, which has a high demand for glucose. The vehicle-treated group and the bevacizumab-treated group had similar tumor uptake (6.16 ± 0.15 vs. 6.32 ± 1.46%ID/g,

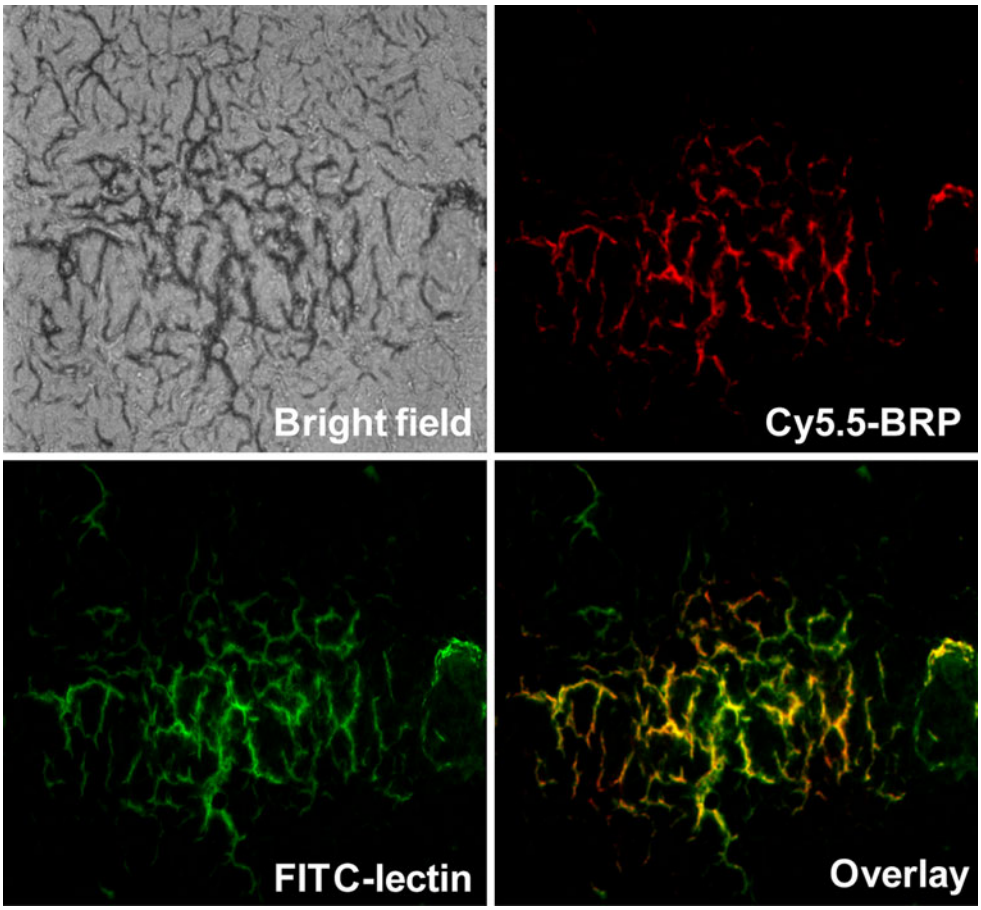

Fig. 3 Microscopic localization of Cy5.5-BRP in bevacizumab-treated LS174T tumor mice. Animals were injected with 1 nmol of Cy5.5-BRP, followed by FITC-conjugated tomato lectin for in vivo dual staining of tumor vasculature. Cy5.5 fluorescence staining of tumor vasculature and FITC staining of tumor vasculature were acquired separately by fluorescence microscopy and then overlaid using MetaMorph imaging processing software. BRP peptide binds specifically to bevacizumab-treated microvascular tumor endothelium cells

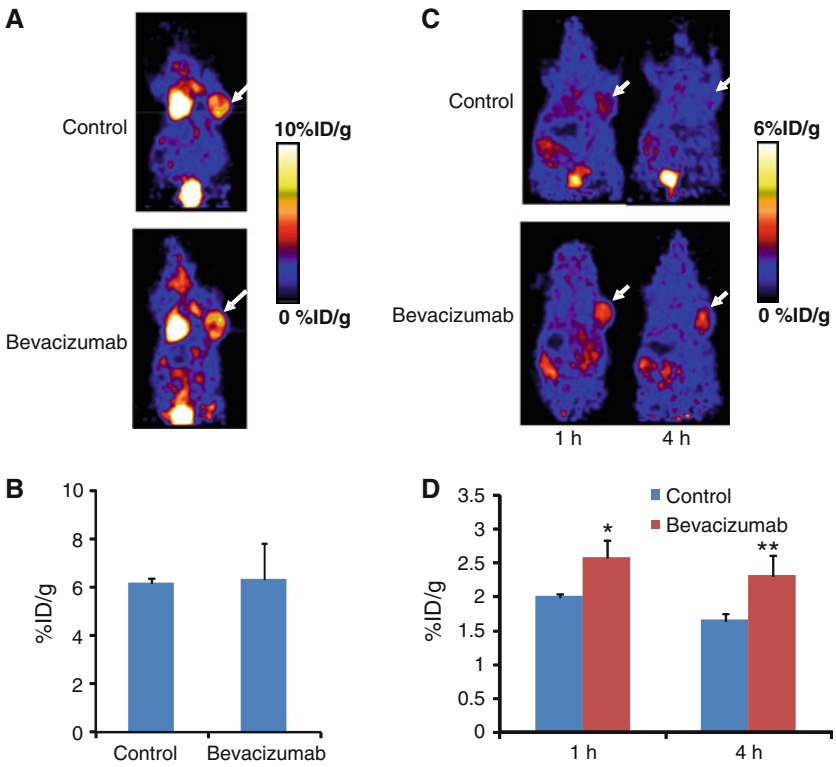

Fig. 4 **a** Representative coronal PET images of LS174T tumor mice at 1 h after intravenous injection of ^{18}F-FDG. **b** ROI analysis of ^{18}F-FDG images showed no difference in tumor uptake (%ID/g) between the saline control and bevacizumab treatment groups. **c** Representative whole-body coronal PET images of LS174T tumor-bearing mice at 1 and 4 h after intravenous injection of ^{18}F-FP-BRP (100 μCi/mouse) with or without bevacizumab treatment. **d** Quantitative PET images of the tumor ROI showed significantly higher tumor uptake of ^{18}F-FP-BRP in bevacizumab-treated versus saline control mice. Tumors are indicated by *arrows*, where $^{*}P < 0.05$, $^{**}P < 0.01$ ($n = 5$ per group)

P = NS) (Fig. 4a, b), indicating that the tumor cells remained viable during this early period of bevacizumab treatment.

By contrast, the LS174T tumor uptake of ^{18}F-FP-BRP increased from 2.02 ± 0.04%ID/g (control) to 2.63 ± 0.25%ID/g (bevacizumab) at 1 h and from 1.59 ± 0.11%ID/g (control) to 2.42 ± 0.30%ID/g (bevacizumab) at the 4-h time point ($P < 0.05$ for both time points) (Fig. 4c, d). The increase in tumor uptake of ^{18}F-FP-BRP is indicative of positive response to bevacizumab treatment.

Discussion

Tumor vascular beds in different phases of anti-angiogenic treatment are morphologically and functionally different (Jain 2001, 2005; Winkler et al. 2004; Tong et al. 2004), which might also suggest changes in molecular expression, or the appearance of new molecules. If these specific biomarkers can be found, it will help us to identify responsive patients and optimal doses, to validate mechanistic hypotheses, to predict efficacy of treatment regimens, and to detect and prevent tumor escape (Jain et al. 2006). Identification of tumor vascular markers has progressed slowly, at least partially because of difficulties in isolating pure populations of endothelial cells from tumor tissues. Moreover, isolated and cultured cells may lose their tissue-specific traits upon culture (Borsum et al. 1982; Augustin et al. 1994). Thus, the phenotype of endothelial cells is unstable and likely to change when the cells are removed from their tumor microenvironments.

Phage display is a very useful technique to obtain defined peptide sequences that interact with a particular molecule. The application of phage display to discover tumor-homing peptides has been reported (Seung-Min et al. 2009). One of the most exciting recent developments has been the use of in vivo phage display to yield disease-specific or organ-specific phage clones (Pasqualini and Ruoslahti 1996; Rajotte et al. 1998). Phage-displayed peptides recovered from irradiated tumors have also been used to assess cancer response to irradiation therapy (Han et al. 2008; Hallahan et al. 2003).

In this study, we used in vivo phage display to screen and identify a linear 12-mer phage peptide sequence that binds specifically to tumor vascular beds subjected to effective bevacizumab treatment. This peptide, when coupled with fluorescent dyes such as Cy5.5 or IRDye800 for NIR fluorescence imaging, or labeled with ^{18}F through a prosthetic labeling group ^{18}F-2-fluoroproprionate (^{18}F-FP), showed significantly higher accumulation in bevacizumab-treated LS174T colorectal cancer model, which secretes high levels of human VEGF. A scrambled peptide used as a control, on the other hand, showed rapid renal clearance and no tumor accumulation in LS174T tumors treated with either vehicle control or bevacizumab. The change in peptide uptake preceded anatomical changes that could be

measured by caliper. ^{18}F-FDG uptake, and hence glucose metabolism, failed to disclose a difference between the control- and bevacizumab-treated LS174T tumors, implying that the viability of the tumor cells was essentially unaltered after bevacizumab exposure. It is of note that we were able to visualize a difference in tumor uptake of BRP 24 h after the third dose of bevacizumab treatment (i.e., the fifth day after bevacizumab treatment began), yet no difference in tumor volume was seen. Statistically significant changes in tumor volume between the bevacizumab-treated group and saline control group were not observed until an additional 5–6 days after the imaging studies showed the uptake of BRP. Such findings in rodents, when translated to humans, may be equivalent to detecting changes in tumors a few months earlier than might be possible using CT or MRI to detect changes in tumor size.

Our data indicate that BRP binds specifically to tumor endothelial cells exposed to bevacizumab, but not to untreated ones. The increase of BRP binding is predictive of effective bevacizumab treatment, but the exact target of this BRP sequence is still unknown. The same sequence has been previously reported to be related to hypoxia (Hardy et al. 2007). Our future efforts will involve the identification of the particular endothelial biomarker protein that recognizes BRP. After the marker is found, we will attempt to optimize the peptide sequence for receptor targeting and detection sensitivity. A further limitation of our study is that we have only tested the response of BRP peptide to bevacizumab treatment. It is imperative to study whether this peptide can also be generalized to evaluate the efficacy of other anti-angiogenic treatments.

In conclusion, we have identified a linear 12-mer peptide, LLADTTHHRPWT, from a phage display that, when conjugated with near-infrared fluorescent dyes or radionuclides, has the ability to selectively bind to bevacizumab-treated tumors but not the untreated tumors. Rapid and non-invasive assessments of pharmacodynamic response by peptides such as this promise to accelerate drug development and to allow early prediction of treatment efficacy.

Acknowledgments This project was supported, in part, by National Cancer Institute (NCI) (P50 CA114747, U54 CA119367, and R24 CA93862) and the Intramural Research Program, NIBIB, NIH. G. Niu is an Imaging Sciences Training Fellowship jointly supported by the Radiology and Imaging Sciences Department, Clinical Center and the Intramural Research Program, NIBIB, NIH. We acknowledge Dr. Henry S. Eden for proof-reading this manuscript.

References

Arap W, Pasqualini R, Ruoslahti E (1998) Cancer treatment by targeted drug delivery to tumor vasculature in a mouse model. Science 279:377–380

Augustin HG, Kozian DH, Johnson RC (1994) Differentiation of endothelial cells: analysis of the constitutive and activated endothelial cell phenotypes. Bioessays 16:901–906

Atkinson AJ, Colburn WA, DeGruttola VG, DeMets DL, Downing GJ, Hoth DF, Oates JA, Peck CC, Schooley RT, Spilker RA, Woodcock J, Zeger SL (2001) Biomarkers and surrogate endpoints: preferred definitions and conceptual framework. Clin Pharmacol Ther 69:89–95

Borsum T, Hagen I, Henriksen T, Carlander B (1982) Alterations in the protein composition and surface structure of human endothelial cells during growth in primary culture. Atherosclerosis 44:367–378

Browder T, Butterfield CE, Kraling BM, Shi B, Marshall B, O'Reilly MS, Folkman J (2000) Antiangiogenic scheduling of chemotherapy improves efficacy against experimental drug-resistant cancer. Cancer Res 60:1878–1886

Ferrara N (2004) Vascular endothelial growth factor: basic science and clinical progress. Endocr Rev 25:581–611

Fox WD, Higgins B, Maiese KM, Drobnjak M, Cordon-Cardo C, Scher HI, Agus DB (2002) Antibody to vascular endothelial growth factor slows growth of an androgen-independent xenograft model of prostate cancer. Clin Cancer Res 8:3226–3231

Fujio Y, Walsh K (1999) Akt mediates cytoprotection of endothelial cells by vascular endothelial growth factor in an anchorage-dependent manner. J Biol Chem 274:16349–16354

Gambhir SS, Czernin J, Schwimmer J, Silverman DH, Coleman RE, Phelps ME (2001) A tabulated summary of the FDG PET literature. J Nucl Med 42:1S–93S

Hallahan D, Geng L, Qu S, Scarfone C, Giorgio T, Donnelly E, Gao X, Clanton J (2003) Integrin-mediated targeting of drug delivery to irradiated tumor blood vessels. Cancer Cell 3:63–74

Han Z, Fu A, Wang H, Diaz R, Geng L, Onishko H, Hallahan DE (2008) Noninvasive assessment of cancer response to therapy. Nat Med 14:343–349

Hardy B, Raiter A, Weiss C, Kaplan B, Tenenbaum A, Battler A (2007) Angiogenesis induced by novel peptides selected from a phage display library by screening human vascular endothelial cells under different physiological conditions. Peptides 28:691–701

Hlatky L, Hahnfeldt P, Folkman J (2002) Clinical application of antiangiogenic therapy: microvessel density, what it does and doesn't tell us. J Natl Cancer Inst 94:883–893

Holash J, Maisonpierre PC, Compton D, Boland P, Alexander CR, Zagzag D, Yancopoulos GD, Wiegand SJ (1999) Vessel cooption, regression, and growth in tumors mediated by angiopoietins and VEGF. Science 284:1994–1998

Hsu AR, Hou LC, Veeravagu A, Greve JM, Vogel H, Tse V, Chen X (2006) In vivo near-infrared fluorescence imaging of integrin alphavbeta3 in an orthotopic glioblastoma model. Mol Imaging Biol 8:315–323

Hu L, Hofmann J, Zaloudek C, Ferrara N, Hamilton T, Jaffe RB (2002) Vascular endothelial growth factor immunoneutralization plus Paclitaxel markedly reduces tumor burden and ascites in athymic mouse model of ovarian cancer. Am J Pathol 161:1917–1924

Hughes MS, Marsh JN, Zhang H, Woodson AK, Allen JS, Lacy EK, Carradine C, Lanza GM, Wickline SA (2006) Characterization of digital waveforms using thermodynamic analogs: detection of contrast-targeted tissue in vivo. IEEE Trans Ultrason Ferroelectr Freq Control 53:1609–1616

Hurwitz H, Fehrenbacher L, Novotny W, Cartwright T, Hainsworth J, Heim W, Berlin J, Baron A, Griffing S, Holmgren E, Ferrara N, Fyfe G, Rogers B, Ross R, Kabbinavar F (2004) Bevacizumab plus irinotecan, fluorouracil, and leucovorin for metastatic colorectal cancer. N Engl J Med 350:2335–2342

Jaffe CC (2006) Measures of response: RECIST, WHO, and new alternatives. J Clin Oncol 24:3245–3251

Jain RK (1998) The next frontier of molecular medicine: delivery of therapeutics. Nat Med 4:655–657

Jain RK (2001) Normalizing tumor vasculature with anti-angiogenic therapy: a new paradigm for combination therapy. Nat Med 7:987–989

Jain RK (2005) Normalization of tumor vasculature: an emerging concept in antiangiogenic therapy. Science 307:58–62

Jain RK, Duda DG, Clark JW, Loeffler JS (2006) Lessons from phase III clinical trials on anti-VEGF therapy for cancer. Nat Clin Pract Oncol 3:24–40

Kelly KA, Waterman P, Weissleder R (2006) In vivo imaging of molecularly targeted phage. Neoplasia 8:1011–1018

Kerbel RS (2006) Antiangiogenic therapy: a universal chemosensitization strategy for cancer? Science 312:1171–1175

Li ZB, Wu Z, Chen K, Ryu EK, Chen X (2008) 18F-labeled BBN-RGD heterodimer for prostate cancer imaging. J Nucl Med 49:453–461

Liu Z, Yan Y, Chin FT, Wang F, Chen X (2009) Dual integrin and gastrin-releasing peptide receptor targeted tumor imaging using (18)F-labeled PEGylated RGD-bombesin heterodimer (18)F-FB-PEG(3)-Glu-RGD-BBN. J Med Chem 52:425–432

Miller KD, Soule SE, Calley C, Emerson RE, Hutchins GD, Kopecky K, Badve S, Storniolo A, Goulet R, Sledge GW Jr (2005) Randomized phase II trial of the anti-angiogenic potential of doxorubicin and docetaxel; primary chemotherapy as Biomarker Discovery Laboratory. Breast Cancer Res Treat 89:187–197

Padhani AR (2003) MRI for assessing antivascular cancer treatments. Br J Radiol 76(Spec No. 1):S60–S80

Pasqualini R, Ruoslahti E (1996) Organ targeting in vivo using phage display peptide libraries. Nature 380:364–366

Rajotte D, Arap W, Hagedorn M, Koivunen E, Pasqualini R, Ruoslahti E (1998) Molecular heterogeneity of the vascular endothelium revealed by in vivo phage display. J Clin Invest 102:430–437

Seung-Min L, Gil-Suk Y, Eun-Sang Y, Tae-Gyun K, In-San K, Byung-Heon L (2009) Application of phage display to discovery of tumor-specific homing peptides: developing strategies for therapy and molecular imaging of cancer. Methods Mol Biol 512:355–363

Sweeney CJ, Miller KD, Sissons SE, Nozaki S, Heilman DK, Shen J, Sledge GW Jr (2001) The antiangiogenic property of docetaxel is synergistic with a recombinant humanized monoclonal antibody against vascular endothelial growth factor or 2-methoxyestradiol but antagonized by endothelial growth factors. Cancer Res 61:3369–3372

Tong RT, Boucher Y, Kozin SV, Winkler F, Hicklin DJ, Jain RK (2004) Vascular normalization by vascular endothelial growth factor receptor 2 blockade induces a pressure gradient across the vasculature and improves drug penetration in tumors. Cancer Res 64:3731–3736

Tozer GM (2003) Measuring tumour vascular response to antivascular and antiangiogenic drugs. Br J Radiol 76(Spec No. 1):S23–S35

Willett CG, Boucher Y, di Tomaso E, Duda DG, Munn LL, Tong RT, Chung DC, Sahani DV, Kalva SP, Kozin SV, Mino M, Cohen KS, Scadden DT, Hartford AC, Fischman AJ, Clark JW, Ryan DP, Zhu AX, Blaszkowsky LS, Chen HX, Shellito PC, Lauwers GY, Jain RK (2004) Direct evidence that the VEGF-specific antibody bevacizumab has antivascular effects in human rectal cancer. Nat Med 10:145–147

Winkler F, Kozin SV, Tong RT, Chae SS, Booth MF, Garkavtsev I, Xu L, Hicklin DJ, Fukumura D, di Tomaso E, Munn LL, Jain RK (2004) Kinetics of vascular normalization by VEGFR2 blockade governs brain tumor response to radiation: role of oxygenation, angiopoietin-1, and matrix metalloproteinases. Cancer Cell 6:553–563

Wu Y, Cai W, Chen X (2006) Near-infrared fluorescence imaging of tumor integrin alpha v beta 3 expression with Cy7-labeled RGD multimers. Mol Imaging Biol 8:226–236